

Prospects for Axion Dark Matter Searches at LISA-like Interferometers

Yue-Hui Yao^{a,c}, Tingyuan Jiang^{a,c}, and Yong Tang^{a,b,c}

^a*University of Chinese Academy of Sciences (UCAS), Beijing 100049, China*

^b*School of Fundamental Physics and Mathematical Sciences,*

Hangzhou Institute for Advanced Study, UCAS, Hangzhou 310024, China

^c*International Center for Theoretical Physics Asia-Pacific, Beijing, China*

Abstract

Axion or axion-like particle has been one of the leading candidates for dark matter. Due to its tiny coupling with photon, axion dark matter in the background can induce distinct phase velocities of light with different parity, an effect known as axion-induced birefringence. Here, we propose a modification to the polarization state of the inter-spacecraft laser link in LISA-like interferometers in space to make them sensitive to this birefringence effect. We discuss the prospects of using Sagnac combinations to search for axion dark matter and derive the corresponding sensitivity. With this setup, we show that next-generation laser interferometers in space would have great sensitivities on the axion-photon coupling with axion mass around 10^{-19} eV \sim 10^{-14} eV.

I. INTRODUCTION

Despite its universal gravitational interaction, the nature of dark matter (DM) remains elusive. Among the various DM candidates, theoretically well-motivated axions [1–6] and, more generally, axion-like particles (ALPs) [7–9] have gained long-standing attention. They can be produced in the early universe through various mechanisms and may offer potential solutions to small-scale problems in the Λ CDM [10–13].

One important feature of axions ¹ is their coupling to gauge bosons, particularly photons [14]. This interaction induces photon-axion conversion in the presence of a background magnetic field, with profound implications in astrophysics, such as spectral distortion [15, 16] and rapid stellar cooling [17, 18]. It also serves as the working principle for many ground-based experiments, such as CAST [19] and “light shining through a wall” [20].

Another key prediction of axion-photon coupling is that light with different parity exhibits distinct phase velocities in axion background, a phenomenon known as birefringence. One result of this difference in phase velocities is the rotation of the polarization plane of linearly polarized light as it propagates through the field. Many experiments leverage this effect, including those using ground-based cavities [21–26] and polarized light from celestial bodies [27–33].

An interferometer equipped with modern photonics technology is also well-suited to detect this difference in phase velocity ², as it can measure light phase with exceptional precision. Here, we investigate the prospects for searching for axion DM in LISA-like space-based gravitational-wave interferometers [46–49]. The main idea is to replace the linearly polarized light in the inter-spacecraft laser link with circularly polarized light and utilize laser noise-free Sagnac combinations to search for axion signals. With this modification, we show that LISA-like detectors will be sensitive to axion-induced birefringence. We estimate the sensitivities of these interferometers and compare them with existing constraints. We find that LISA-like interferometers can be more sensitive to axion-photon coupling than the existing limits in some mass range. In particular, interferometers with better noise level, such as BBO, could improve by several orders of magnitude across a broad range of masses.

The paper is organized as follows. In section II, we present the theoretical framework related to the axion-induced birefringence effect. In section III, we describe the structure of

¹ Hereafter, we use “axions” to collectively refer to both axions and axion-like particles.

² DM may also leave traces in interferometers through other different mechanisms [34–45].

LISA-like detectors and time-delay interferometry. We then discuss the single link response with circularly polarized laser in section III A, and linearly polarized laser in section III B. In section IV, we provide a detailed description of the proposed modification and the use of Sagnac combinations to search for axion signals. In section V, we derive the sensitivities of the interferometers, compare them with existing bounds, and investigate the factors limiting sensitivity. Finally, we conclude in section VI.

In this paper, we use natural units $c = \hbar = 1$ and the metric $g_{\mu\nu} = (+, -, -, -)$.

II. AXION-INDUCED BIREFRINGENCE

In this section, we present the theoretical framework for the birefringence effect arising from axion-photon interactions as electromagnetic waves propagate through the axion field.

The Lagrangian describing the Chern-Simons interaction between the axion and photon field is given by [50–52]

$$\mathcal{L} = -\frac{1}{4}F_{\mu\nu}F^{\mu\nu} + \frac{1}{2}\partial_\mu a \partial^\mu a - \frac{1}{2}m^2 a^2 - \frac{g_{a\gamma}}{4}aF_{\mu\nu}\tilde{F}^{\mu\nu}, \quad (1)$$

where a is the axion field with mass m , $F^{\mu\nu}$, $\tilde{F}^{\mu\nu} = \frac{1}{2}\epsilon^{\mu\nu\rho\sigma}F_{\rho\sigma}$ are the electromagnetic field tensor and its dual tensor, respectively, and $g_{a\gamma}$ is the coupling between axion and photon. The equations of motion for the fields are derived as

$$\partial_\beta F^{\beta\alpha} = -g_{a\gamma}\partial_\mu a \tilde{F}^{\mu\alpha}, \quad (2)$$

$$(\partial_\mu \partial^\mu + m^2)a = -\frac{g_{a\gamma}}{4}F_{\mu\nu}\tilde{F}^{\mu\nu}, \quad (3)$$

which can also be expressed explicitly in terms of the electric and magnetic fields

$$\nabla \cdot \mathbf{E} = -g_{a\gamma}\nabla a \cdot \mathbf{B}, \quad (4)$$

$$\frac{\partial \mathbf{E}}{\partial t} - \nabla \times \mathbf{B} = -g_{a\gamma}\left(\frac{\partial a}{\partial t} \cdot \mathbf{B} + \nabla a \times \mathbf{E}\right), \quad (5)$$

$$(\partial_\mu \partial^\mu + m^2)a = g_{a\gamma}\mathbf{E} \cdot \mathbf{B}. \quad (6)$$

Given that the laser power in the interferometer is only about a few watts and $a \sim \sqrt{2\rho_{\text{DM}}}/m$, where $\rho_{\text{DM}} \approx 0.4 \text{ GeV}/\text{cm}^3$ is the local DM energy density, we can neglect the back-action of light on the axion field and set the right-hand side of Eq. (6) to zero. The homogeneous Klein-Gordon equation has a plane-wave solution $e^{i(\omega_a t - \mathbf{k}_a \cdot \mathbf{x} + \theta_a)}$, where

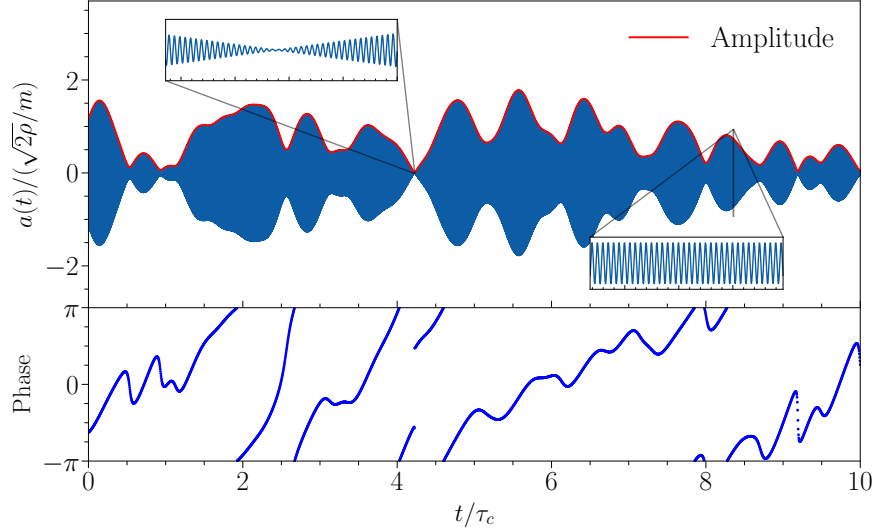


FIG. 1. The evolution of the axion field at a fixed spatial point. The amplitude and phase vary stochastically over the coherence time τ_c . The two inset plots show the Compton oscillation.

$\omega_a \simeq m(1 + \mathbf{v}^2/2)$ and $\mathbf{k}_a \simeq m\mathbf{v}$, describing the collective motion of axion particles with velocity \mathbf{v} . Since DM particles near the solar system exhibit a range of velocities, the axion field can be represented as a superposition of monochromatic plane waves corresponding to axion particles with varying velocities. The behavior of the axion field can be described by [53, 54]

$$a(\mathbf{x}, t) = a_0(\mathbf{x}, t) \cos[mt + \theta_0(\mathbf{x}, t)], \quad (7)$$

where the amplitude $a_0(\mathbf{x}, t)$ and phase $\theta_0(\mathbf{x}, t)$ vary stochastically on scales set by the coherence time τ_c and coherence length λ_c

$$\tau_c = \frac{2\pi}{m\sigma^2} \approx 4.13 \times 10^8 \text{s} \left(\frac{10^{-17} \text{eV}}{m} \right), \quad (8)$$

$$\lambda_c = \frac{2\pi}{m\sigma} \approx 1.24 \times 10^{11} \text{km} \left(\frac{10^{-17} \text{eV}}{m} \right), \quad (9)$$

where $\sigma \simeq 10^{-3}$ is the velocity dispersion of DM. Figure. 1 illustrates the evolution of the axion field at a fixed spatial point.

We can make further simplifications. Since axion considered here has a coherence length much longer than the interferometer's arm length and a coherence time exceeding the observation duration, we can neglect the spatial and temporal dependence of the amplitude and phase, and Eq. (7) reduces to

$$a(t) = a_0 \cos(mt + \theta_0) = a_0 e^{i(mt + \theta_0)}. \quad (10)$$

Combining Eqs. (4, 5) with the homogeneous Maxwell equations³ and neglecting all gradient terms, we obtain the wave equations

$$\left(\frac{\partial^2}{\partial t^2} - \nabla^2\right) \mathbf{E} = g_{a\gamma} (\dot{a}\nabla \times \mathbf{E} - \ddot{a}\mathbf{B}), \quad (11)$$

$$\left(\frac{\partial^2}{\partial t^2} - \nabla^2\right) \mathbf{B} = g_{a\gamma} \dot{a}\nabla \times \mathbf{B}. \quad (12)$$

Since the laser's angular frequency satisfies $\omega \sim \mathcal{O}(\text{eV}) \gg m$ and $\ddot{a}\mathbf{B}/\dot{a}\nabla \times \mathbf{E} \sim m/\omega$, we can neglect the term $\ddot{a}\mathbf{B}$ in Eq. (11), and the wave equations share the same form. We exemplify the birefringence effect with the electric field in the following discussion.

The condition $m \ll \omega$ also implies the existence of a sufficiently small spacetime region where \dot{a} can be treated as static, and Eq. (11) admits a monochromatic plane-wave solution

$$\mathbf{E} = \sum_{j=\pm} E_j e^{i(\omega t - \mathbf{k}\cdot\mathbf{x})} \boldsymbol{\epsilon}_j(\hat{\mathbf{k}}), \quad (13)$$

where E_j are complex amplitudes and $\boldsymbol{\epsilon}_{\pm}$ are the circularly polarized basis satisfying $i\hat{\mathbf{k}} \times \boldsymbol{\epsilon}_{\pm}(\hat{\mathbf{k}}) = \pm\boldsymbol{\epsilon}_{\pm}(\hat{\mathbf{k}})$. Substituting Eq. (13) into Eq. (11), we have the dispersion relations

$$\omega^2 - k^2 = \pm g_{a\gamma} \dot{a} k. \quad (14)$$

Consequently, the phase velocities of circularly polarized light are given by

$$v_{\pm} = \frac{\omega}{k} \simeq 1 \pm \frac{g_{a\gamma} \dot{a}}{2\omega}. \quad (15)$$

Therefore, the left circularly polarized (LCP) and right circularly polarized (RCP) light⁴ are the eigenstates of the axion medium, exhibiting distinct phase velocities as they propagate through it. This effect is known as birefringence.

III. SIGNAL RESPONSE OF INTERFEROMETER

In this section, we first briefly describe the basic operational principles of LISA-like space-based interferometers. We then derive the response of signal in a single link, assuming that the light is either linearly polarized (LP) or circularly polarized (CP). The main conclusion

³ The homogeneous Maxwell equations are expressed by the Bianchi identities $\partial_{\mu} \tilde{F}^{\mu\nu} = 0$ and remain unaltered by the axion-photon coupling.

⁴ The definitions of LCP and RCP vary among literature. In this work, we refer to $\boldsymbol{\epsilon}_{+}$ as LCP, as the directions of rotation of \mathbf{E} and the light's propagation are related by the left-hand rule.

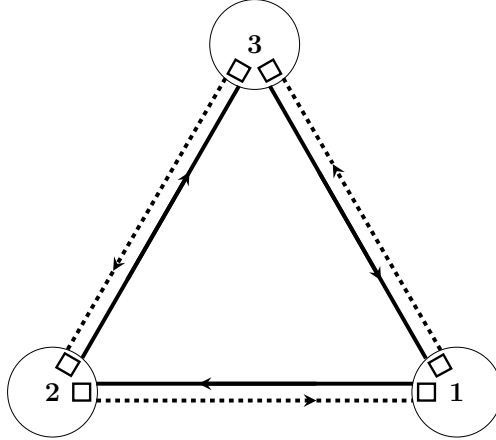


FIG. 2. Schematic representation of LISA. Each spacecraft is equipped with two optical benches. Each spacecraft sends and receives laser beams from the other two, forming three clockwise links and three counterclockwise links.

is that LISA-like interferometers with the current design are insensitive to axion-induced birefringence.

The LISA-like interferometer typically consists of three spacecrafts, forming a quasi-equilateral triangle configuration in space with arm lengths of approximately $\mathcal{O}(10^6\text{km})$ for the heliocentric orbit or $\mathcal{O}(10^5\text{km})$ for the geocentric orbit. Each spacecraft contains two optical benches, each hosting a free-falling test mass. Every spacecraft sends and receives laser beams from the other two. The laser from a distant spacecraft interferes with the local laser, forming a beat note whose phase is related to the light travel time between the two spacecrafts. Consequently, the three spacecrafts result in six laser links with three clockwise and three counterclockwise, as shown in Fig. 2.

Given the current stability of laser, the single-link data will be overwhelmed by laser noise. Furthermore, due to the orbital motion of the spacecraft, the lengths of the interferometer's arms are unequal and evolve annually, rendering the simple Michelson interferometric configuration invalid. To address these challenges, we employ the time-delay interferometry (TDI) [55] to synthesize virtual interferometric configurations that have light paths of nearly equal length by combining the time-shifted single-link data. Since the building blocks of any TDI combination are the single-link responses, we will begin with a detailed study of the single-link's response to the axion field.

A. Circularly polarized light

We start with the case of CP light. Assuming that the light is CP when it leaves the sending spacecraft, the time ΔT_{\pm} taken by the light to reach the receiving spacecraft at time t is given by

$$L = \int_{t-\Delta T_{\pm}}^t dt v_{\pm} = \Delta T_{\pm} \pm \frac{g_{a\gamma}}{2\omega} [a(t) - a(t - \Delta T_{\pm})], \quad (16)$$

where L is the arm length of the interferometer. Keeping the leading order in $g_{a\gamma}$, we have

$$\Delta T_{\pm} \simeq L \mp \frac{g_{a\gamma}}{2\omega} [a(t) - a(t - L)]. \quad (17)$$

The relative frequency fluctuation of the laser induced by the axion field is given by

$$\eta_{rs}(t) = -\frac{d(\Delta T_{\pm})}{dt} = \pm \frac{img_{a\gamma}}{2\omega} [a(t) - a(t - L)], \quad (18)$$

where the subscripts $r, s = 1, 2, 3$ denote the indices of the spacecraft.

Note that the axion signal in Eq. (18) does not depend on the propagation direction of light but only on the difference in the axion field at the emission and reception times. This is a manifestation of the topological nature of the Chern-Simons interaction in Eq. (1). This should be contrasted with the scenario where the signal is related to a vector field or the gradient of a scalar field. In that case, the signal involves the scalar product of the field gradient or vector field with the arm's direction vector, i.e., $\hat{\mathbf{n}} \cdot \nabla a$ or $\hat{\mathbf{n}} \cdot \mathbf{A}$, indicating that the signal is direction-dependent and will vary annually due to the orbital motion of the constellation [56–59].

B. Linearly polarized light

Now, we turn to the case where light is LP when it leaves the spacecraft, which reflects the current design of LISA-like detectors. Without loss of generality, we assume that the light is x -polarized (horizontally polarized, HP) in the absence of the axion field. The schematic plot of the light path is shown in Fig. 3. The x -polarized light is described by the Jones vector [60]

$$\mathbf{E}_e(t) = \begin{bmatrix} 1 \\ 0 \end{bmatrix} e^{i\omega t} = \begin{bmatrix} 1 \\ i \end{bmatrix} \frac{e^{i\omega t}}{2} + \begin{bmatrix} 1 \\ -i \end{bmatrix} \frac{e^{i\omega t}}{2}, \quad (19)$$

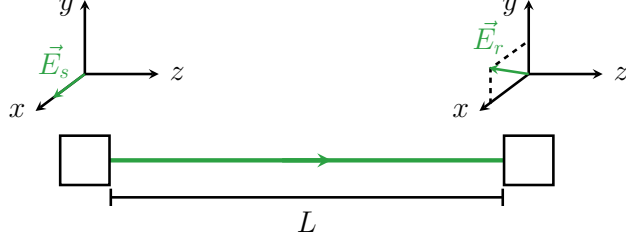


FIG. 3. Schematic representation of the light path for a single link under the current design. Light is horizontally polarized upon leaving the sending spacecraft. As it travels through the axion dark matter background, the polarization angle rotates, developing a vertically polarized component.

where we expand it into the CP basis. Then, according to Eq. (17), the electric field received by the other spacecraft at time t is

$$\mathbf{E}_r(t) = \begin{bmatrix} 1 \\ i \end{bmatrix} \frac{e^{i\omega(t-\Delta T_+)}}{2} + \begin{bmatrix} 1 \\ -i \end{bmatrix} \frac{e^{i\omega(t-\Delta T_-)}}{2}. \quad (20)$$

We can read out the components of \mathbf{E}_r in the LP basis directly,

$$\begin{aligned} E_x &= \frac{\cos[\omega(t-\Delta T_+)] + \cos[\omega(t-\Delta T_-)]}{2} \\ &= \cos\left(\omega \frac{\Delta T_- - \Delta T_+}{2}\right) \cos\left[\omega\left(t - \frac{\Delta T_- + \Delta T_+}{2}\right)\right] \\ &= \cos\left[g_{a\gamma} \frac{a(t) - a(t-L)}{2}\right] \cos[\omega(t-L)], \end{aligned} \quad (21)$$

$$\begin{aligned} E_y &= \frac{-\sin[\omega(t-\Delta T_+)] + \sin[\omega(t-\Delta T_-)]}{2} \\ &= -\sin\left(\omega \frac{\Delta T_- - \Delta T_+}{2}\right) \cos\left[\omega\left(t - \frac{\Delta T_- + \Delta T_+}{2}\right)\right] \\ &= -\sin\left[g_{a\gamma} \frac{a(t) - a(t-L)}{2}\right] \cos[\omega(t-L)]. \end{aligned} \quad (22)$$

Equations. (21, 22) indicate that when traveling through the axion field, the polarization angle of the received light varies periodically. This variation in polarization angle produces a vertically polarized (VP) component, which serves as a target for many experiments [22, 24–26, 28, 31]. However, the current design of LISA-like interferometers is not sensitive to the evolution of the polarization angle but rather to the phase of the HP component. From Eq. (21), while the axion field causes the amplitude of the HP component to experience periodic modulation at $\mathcal{O}(g_{a\gamma}^2)$, it leaves the phase intact compared to the vacuum case. Therefore, within the current design, LISA-like interferometers are insensitive to axion-induced birefringence.

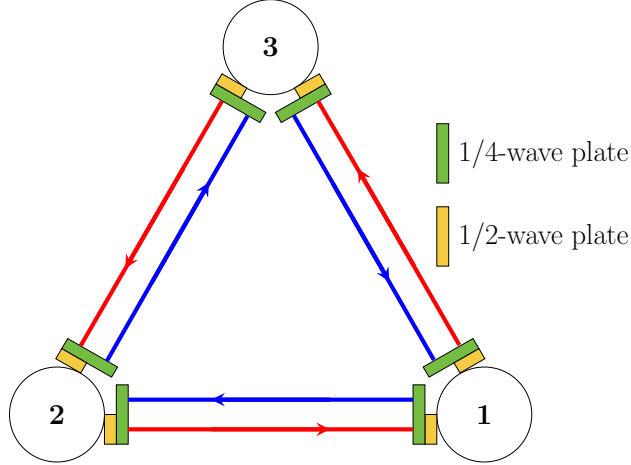


FIG. 4. Schematic representation of the modified light path, with the blue and red lines indicating left circularly polarized light and right circularly polarized light, respectively. Compared to the original design, the linearly polarized light in inter-spacecraft laser link is replaced with left circularly polarized light (right circularly polarized light) for clockwise (counterclockwise) links.

There are two approaches to make the interferometer sensitive to axion-induced birefringence. One approach involves replacing the current polarization-insensitive design with a polarization-sensitive design [22, 24], allowing the GW interferometer to search for the variations in the polarization angle. The second approach is to substitute the LP light transmitted between spacecrafts with CP light [61]. In the following discussion, we will focus on the latter possibility.

IV. MODIFIED CONFIGURATION AND SAGNAC COMBINATION

The issue can be addressed by replacing the LP light with CP light in the link. This can be achieved by introducing wave plates at suitable positions along the light path. Here, we propose a modification of the light path and the utilization of the laser noise-free Sagnac combinations in TDI to search for axion-induced signals.

The modification is illustrated in Fig. 4. A pair of quarter-wave plate and half-wave plates are added at the ends of each link, which changes the polarization state of the light between horizontally polarized and left circularly polarized (right circularly polarized) when the light travels clockwise (counterclockwise).

To illustrate the effect of this design, we first consider the signal in a clockwise link. The

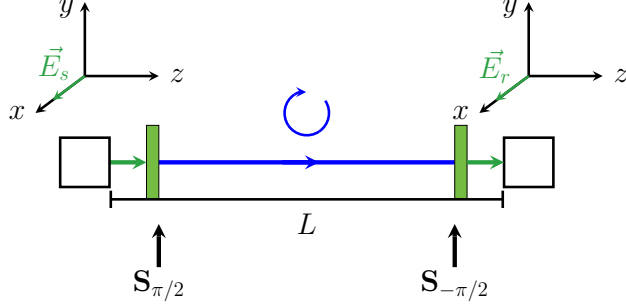


FIG. 5. Schematic representation of the light path for a clockwise link with additional quarter-wave plates. The horizontally polarized light is converted into left circularly polarized light upon leaving the sending spacecraft. Upon reaching the receiving spacecraft, the left circularly polarized is converted back into horizontally polarized light.

light path of the link is shown in Fig. 5. The Jones matrix for the quarter-wave plate near the sending spacecraft is given by

$$\mathbf{S}_{\pi/2} = \frac{1}{\sqrt{2}} \begin{bmatrix} 1 & -1 \\ i & i \end{bmatrix}, \quad (23)$$

which converts the HP light into the LCP light. The Jones matrix for the quarter-wave plate near the receiving spacecraft is given by

$$\mathbf{S}_{-\pi/2} = \frac{1}{\sqrt{2}} \begin{bmatrix} 1 & -i \\ -1 & -i \end{bmatrix}. \quad (24)$$

which converts the LCP light back into the HP light. Since both Jones matrices have $|\det[\mathbf{S}]| = 1$, the laser power is not reduced with the inclusion of these additional wave plates. With this configuration, the electric field received at the end of the link at time t is given by

$$\mathbf{E}_r = \mathbf{S}_{-\pi/2} e^{i\omega(t-\Delta T_+)} \mathbf{S}_{\pi/2} \begin{bmatrix} 1 \\ 0 \end{bmatrix} = \begin{bmatrix} 1 \\ 0 \end{bmatrix} e^{i\omega(t-\Delta T_+)}, \quad (25)$$

where the field is horizontally polarized and has a phase shift $\omega\Delta T_+$.

The counterclockwise link includes an additional half-wave plate, which converts the HP light into VP light. This VP light is then transformed into RCP light by the quarter-wave plate. At the end of the counterclockwise link, the reverse process occurs, resulting in a HP light, but with a phase shift $\omega\Delta T_-$. In fact, this design is analogous to a ring cavity setup. Since the additional phases for the two CP lights differ by a minus sign, and the

output of the Sagnac combinations represents the phase difference between the clockwise and counterclockwise light paths, this configuration will maximize the interferometer's sensitivity to axions.

V. SENSITIVITY

Now we estimate the sensitivity of the Sagnac combination to the axion-photon coupling. The Sagnac α combination is given by

$$\alpha(t) = [\eta_{13} + \eta_{32,2} + \eta_{21,12}] - [\eta_{12} + \eta_{23,3} + \eta_{31,13}], \quad (26)$$

where $\eta(t)_{rs,ij} \equiv \eta_{rs}(t - L_i - L_j)$. Substituting Eq. (18) into Eq. (26) and using the approximation of static and equal arm lengths, i.e. $L_i = L_j$, we have

$$\alpha(t) = \frac{img_{a\gamma}a_0}{\omega} (1 - e^{-im3L}) e^{i(mt+\theta_0)}. \quad (27)$$

The one-sided power spectral density (PSD) of the signal is given by

$$P_s(f) = 2 \frac{|\tilde{\alpha}(f)|^2}{T} = \frac{4\rho_{\text{DM}}g_{a\gamma}^2}{\omega^2} \sin^2(3\pi fL) T, \text{ for } f = f_c; \quad \text{else } P_s(f) = 0, \quad (28)$$

where $f_c = m/2\pi$ is the axion Compton frequency, T is the observation period, and in the last step, we replace a_0^2 with its ensemble average, $\langle a_0^2 \rangle = 2\rho_{\text{DM}}/m^2$.

The signal-to-noise ratio (SNR) is defined as

$$\text{SNR} = \frac{P_s(f)}{P_n(f)}, \quad (29)$$

where $P_n(f)$ is the one-sided PSD of the noise in the Sagnac combinations [42]

$$P_n(f) = 8 [2 \sin^2(\pi fL) + \sin^2(3\pi fL)] S_{\text{acc}}(f) + 6S_{\text{oms}}(f). \quad (30)$$

S_{oms} and S_{acc} denote the optical metrology system noise and test mass acceleration noise, respectively. For LISA, Taiji, and TianQin, they are given by [62]

$$S_{\text{oms}}(f) = \left(\frac{2\pi f}{c} s_{\text{oms}} \right)^2 \left[1 + \left(\frac{2 \times 10^{-3} \text{ Hz}}{f} \right)^4 \right] \frac{1}{\text{Hz}}, \quad (31)$$

$$S_{\text{acc}}(f) = \left(\frac{s_{\text{acc}}}{2\pi f c} \right)^2 \left[1 + \left(\frac{0.4 \times 10^{-3} \text{ Hz}}{f} \right)^2 \right] \left[1 + \left(\frac{f}{8 \times 10^{-3} \text{ Hz}} \right)^4 \right] \frac{1}{\text{Hz}}, \quad (32)$$

	LISA	Taiji	TianQin	BBO
Arm length L (10^9m)	2.5	3	0.17	0.05
s_{oms} (10^{-12}m)	15	8	1	1.4×10^{-5}
s_{acc} ($10^{-15}\text{m} \cdot \text{s}^{-2}$)	3	3	1	3×10^{-2}

TABLE I. The parameters of several planned space-based interferometers. The laser wavelength is 1064nm for LISA, Taiji, and TianQin, and 355nm for BBO [69]. s_{oms} and s_{acc} are the parameters of optical metrology system noise and test mass acceleration noise, respectively.

while for BBO, the frequency-dependent factors in the square brackets are neglected [63]. We define the sensitivity as the coupling strength that results in $\text{SNR} = 1$ within a one-year observation period ⁵. In Fig. 6, we plot the sensitivities of the four interferometers to the axion-photon coupling $g_{a\gamma}$ and compare them with the existing constraints from ground-based CAST experiment [19] and astrophysical observations [15, 16, 65]. The parameters adopted for LISA, Taiji, TianQin, and BBO are summarized in Table. I. Other similar projects, DECIGO [66], LISAmass [67], ASTROD-GW [68] are not listed here.

As shown in Fig. 6, in their most sensitive mass range those interferometers will improve on the existing constraints from CAST [19] and SN1987A [65]. LISA, Taiji, and TianQin could achieve sensitivities of $g_{a\gamma} \sim 3 \times 10^{-13} \text{ GeV}^{-1}$ for axions with mass around 10^{-17} eV . Due to its better noise performance, BBO could achieve $g_{a\gamma} \sim 10^{-16} \text{ GeV}^{-1}$ across a broad mass range, improving the constraints by five orders of magnitude. We also present constraints derived from the spectra of active galactic nuclei [15, 16]. While these constraints are comparable to the sensitivities of LISA, Taiji and TianQin, they rely on theoretical assumption on galactic magnetic models.

Note that for LISA, Taiji, and TianQin, the symmetric structure of the Sagnac combination strongly suppresses the acceleration noise, rendering the optical metrology noise dominant across the entire frequency band, as shown in Fig. 7. Therefore, improving the performance of the optical metrology noise will be crucial to these interferometers' sensitivity to axions.

Neglecting the acceleration noise and working under the low-frequency limit, their sensi-

⁵ We note that the stochastic nature of the field will generally degrade sensitivity [45, 64]. However, the exact degree of degradation depends on the specific relationship between the signal and the field, as well as the statistical framework used. In this context, our $\text{SNR} = 1$ sensitivity serves as an estimate of the interferometer performance.

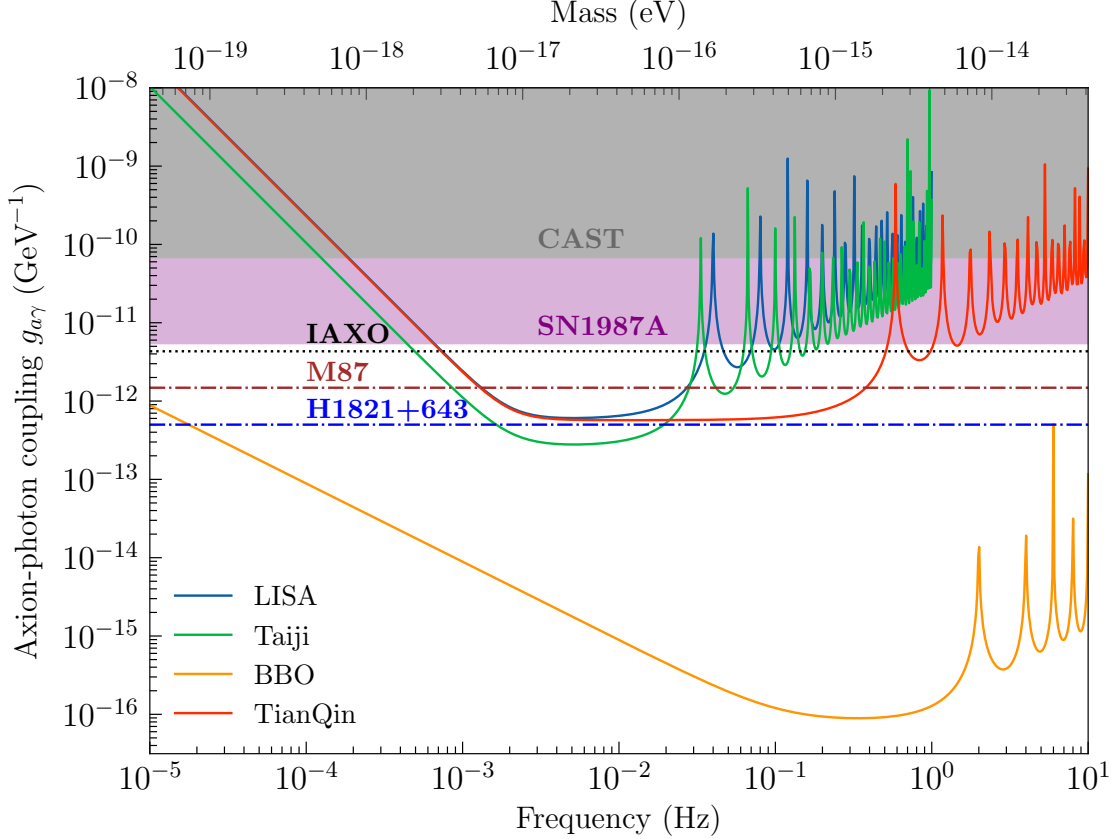


FIG. 6. Sensitivities of several LISA-like interferometers to the axion-photon coupling $g_{a\gamma}$. The bounds from CAST [19] and SN1987A [65] are indicated by the gray and purple shaded areas, respectively. The constraints from astrophysical observations of the M87 galaxy [16] and quasar H1821+643 [15] are shown with dot-dashed lines. The sensitivity of future axion experiments IAXO [70] is also indicated (black dotted).

tivities can be approximated by

$$g_{a\gamma} \simeq \left(\frac{\omega^2 S_{\text{oms}}}{6\pi^2 \rho_{\text{DM}} T} \right)^{1/2} \frac{1}{fL}. \quad (33)$$

Therefore, an interferometer with a longer arm length and lower optical metrology noise exhibits better sensitivity. This also explains why the sensitivities of LISA and TianQin are comparable, while LISA benefits from a longer arm length, TianQin with a lower optical metrology noise. However, the above discussion does not fully apply to BBO. Despite the suppression of acceleration noise in the Sagnac combination, it dominates at low frequencies due to BBO's much improved optical metrology noise, as shown in Fig. 7.

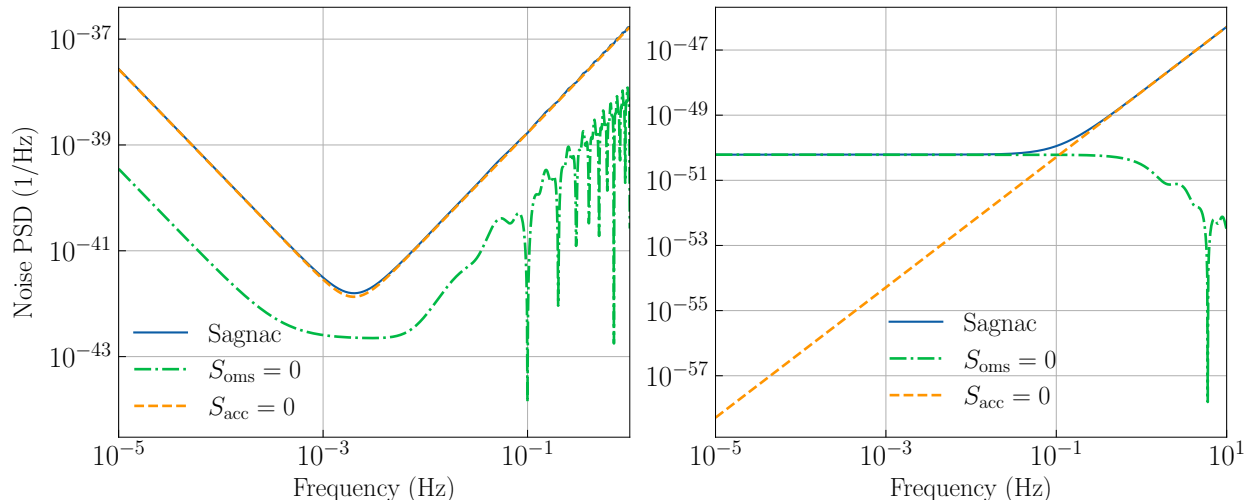


FIG. 7. The noise PSDs in Sagnac combination P_n , Taiji (left) and BBO (right). The blue solid line is the full Sagnac noise PSD, while the orange dashed line and the green dot-dashed line show the cases where $S_{\text{oms}} = 0$ and $S_{\text{acc}} = 0$, respectively.

VI. CONCLUSION

In this work, we propose to adjust LISA-like gravitational-wave laser interferometers in space to make them also sensitive to axion dark matter. This adjustment changes the polarization of the inter-spacecraft laser light from linearly polarized to circularly polarized, leveraging the axion-induced birefringence. We suggest using the Sagnac combinations to search for axion signals and derive the corresponding sensitivity to the axion-photon coupling $g_{a\gamma}$. We show that LISA-like interferometers could probe previously unexplored regions in parameter space. For LISA, Taiji, and TianQin, these interferometers could improve the sensitivity from CAST and SN1987A by an order of the magnitude in the mass range $10^{-17}\text{eV} \sim 10^{-15}\text{eV}$ with a one-year observation. Next generation detector BBO could improve by five orders of magnitude with mass around 10^{-15}eV due to its much better noise control. Our results indicate that with minor modifications, laser interferometers in space could significantly advance axion dark matter search, providing other insight for extending the scientific goals of future gravitational-wave detection missions.

ACKNOWLEDGEMENT

The authors are grateful to Yan Cao and Yu-Feng Zhou for insightful discussions. This work is supported by the National Key Research and Development Program of China (Grant No.2021YFC2201901), and the Fundamental Research Funds for the Central Universities.

Note added: While we were finalizing the manuscript, a preprint [71] discussing similar topics appeared on arXiv.

-
- [1] R. D. Peccei and H. R. Quinn, *Phys. Rev. Lett.* **38**, 1440 (1977).
 - [2] S. Weinberg, *Phys. Rev. Lett.* **40**, 223 (1978).
 - [3] F. Wilczek, *Phys. Rev. Lett.* **40**, 279 (1978).
 - [4] J. Preskill, M. B. Wise, and F. Wilczek, *Phys. Lett. B* **120**, 127 (1983).
 - [5] L. F. Abbott and P. Sikivie, *Phys. Lett. B* **120**, 133 (1983).
 - [6] M. Dine and W. Fischler, *Phys. Lett. B* **120**, 137 (1983).
 - [7] T. Damour and A. M. Polyakov, *General Relativity and Gravitation* **26**, 1171–1176 (1994).
 - [8] T. Damour and A. Polyakov, *Nuclear Physics B* **423**, 532–558 (1994).
 - [9] S. Capozziello and M. De Laurentis, *Physics Reports* **509**, 167–321 (2011).
 - [10] W. J. G. de Blok, *Advances in Astronomy* **2010** (2009), 10.1155/2010/789293.
 - [11] M. Boylan-Kolchin, J. S. Bullock, and M. Kaplinghat, *Monthly Notices of the Royal Astronomical Society: Letters* **415**, L40–L44 (2011).
 - [12] J. S. Bullock and M. Boylan-Kolchin, *Annual Review of Astronomy and Astrophysics* **55**, 343–387 (2017).
 - [13] S. Tulin and H.-B. Yu, *Physics Reports* **730**, 1–57 (2018).
 - [14] F. Chadha-Day, J. Ellis, and D. J. E. Marsh, “Axion dark matter: What is it and why now?” (2022), [arXiv:2105.01406](https://arxiv.org/abs/2105.01406) [hep-ph].
 - [15] J. S. Reynés, J. H. Matthews, C. S. Reynolds, H. R. Russell, R. N. Smith, and M. C. D. Marsh, *Mon. Not. Roy. Astron. Soc.* **510**, 1264 (2021), [arXiv:2109.03261](https://arxiv.org/abs/2109.03261) [astro-ph.HE].
 - [16] M. D. Marsh, H. R. Russell, A. C. Fabian, B. R. McNamara, P. Nulsen, and C. S. Reynolds, *Journal of Cosmology and Astroparticle Physics* **2017**, 036 (2017).
 - [17] M. Giannotti, I. G. Irastorza, J. Redondo, A. Ringwald, and K. Saikawa, *JCAP* **10**, 010

- (2017), [arXiv:1708.02111 \[hep-ph\]](#).
- [18] A. H. Corsico, L. G. Althaus, A. D. Romero, A. S. Mukadam, E. Garcia-Berro, J. Isern, S. O. Kepler, and M. A. Corti, *JCAP* **12**, 010 (2012), [arXiv:1211.3389 \[astro-ph.SR\]](#).
- [19] V. Anastassopoulos *et al.* (CAST), *Nature Phys.* **13**, 584 (2017), [arXiv:1705.02290 \[hep-ex\]](#).
- [20] R. Ballou, G. Deferne, M. Finger, M. Finger, L. Flekova, J. Hosek, S. Kunc, K. Macuchova, K. A. Meissner, P. Pugnati, M. Schott, A. Siemko, M. Slunecka, M. Sulc, C. Weinsheimer, and J. Zicha (OSQAR Collaboration), *Phys. Rev. D* **92**, 092002 (2015).
- [21] A. C. Melissinos, *Phys. Rev. Lett.* **102**, 202001 (2009).
- [22] K. Nagano, T. Fujita, Y. Michimura, and I. Obata, *Phys. Rev. Lett.* **123**, 111301 (2019).
- [23] J. Heinze, A. Gill, A. Dmitriev, J. Smetana, T. Yan, V. Boyer, D. Martynov, H. Grote, J. Lough, A. Ejlli, and G. Müller, *New Journal of Physics* **26**, 055002 (2024).
- [24] J. Heinze, A. Gill, A. Dmitriev, J. c. v. Smetana, T. Yan, V. Boyer, D. Martynov, and M. Evans, *Phys. Rev. Lett.* **132**, 191002 (2024).
- [25] H. Liu, B. D. Elwood, M. Evans, and J. Thaler, *Phys. Rev. D* **100**, 023548 (2019).
- [26] D. Martynov and H. Miao, *Phys. Rev. D* **101**, 095034 (2020).
- [27] M. M. Ivanov, Y. Y. Kovalev, M. L. Lister, A. G. Panin, A. B. Pushkarev, T. Savolainen, and S. V. Troitsky, *JCAP* **02**, 059 (2019), [arXiv:1811.10997 \[astro-ph.CO\]](#).
- [28] T. Liu, G. Smoot, and Y. Zhao, *Phys. Rev. D* **101**, 063012 (2020).
- [29] M. A. Fedderke, P. W. Graham, and S. Rajendran, *Phys. Rev. D* **100**, 015040 (2019).
- [30] A. D. Plascencia and A. Urbano, *JCAP* **04**, 059 (2018), [arXiv:1711.08298 \[gr-qc\]](#).
- [31] T. Fujita, R. Tazaki, and K. Toma, *Phys. Rev. Lett.* **122**, 191101 (2019).
- [32] G.-W. Yuan, Z.-Q. Xia, C. Tang, Y. Zhao, Y.-F. Cai, Y. Chen, J. Shu, and Q. Yuan, *JCAP* **03**, 018 (2021), [arXiv:2008.13662 \[astro-ph.HE\]](#).
- [33] T. Liu, X. Lou, and J. Ren, *Phys. Rev. Lett.* **130**, 121401 (2023).
- [34] A. Aoki and J. Soda, *Int. J. Mod. Phys. D* **26**, 1750063 (2016), [arXiv:1608.05933 \[astro-ph.CO\]](#).
- [35] S. M. Vermeulen *et al.*, (2021), [10.1038/s41586-021-04031-y](#), [arXiv:2103.03783 \[gr-qc\]](#).
- [36] A. Pierce, K. Riles, and Y. Zhao, *Phys. Rev. Lett.* **121**, 061102 (2018).
- [37] R. Abbott *et al.* (LIGO Scientific, KAGRA, Virgo), *Phys. Rev. D* **105**, 063030 (2022), [Erratum: *Phys.Rev.D* 109, 089902 (2024)], [arXiv:2105.13085 \[astro-ph.CO\]](#).
- [38] H.-K. Guo, K. Riles, F.-W. Yang, and Y. Zhao, *Commun. Phys.* **2**, 155 (2019), [arXiv:1905.04316 \[hep-ph\]](#).

- [39] A. L. Miller and L. Mendes, [Phys. Rev. D **107**, 063015 \(2023\)](#).
- [40] H. Nakatsuka, S. Morisaki, T. Fujita, J. Kume, Y. Michimura, K. Nagano, and I. Obata, [Phys. Rev. D **108**, 092010 \(2023\)](#).
- [41] K. Fukusumi, S. Morisaki, and T. Suyama, [Phys. Rev. D **108**, 095054 \(2023\)](#).
- [42] J.-C. Yu, Y.-H. Yao, Y. Tang, and Y.-L. Wu, [Phys. Rev. D **108**, 083007 \(2023\)](#).
- [43] H. Kim, [JCAP **12**, 018 \(2023\)](#), [arXiv:2306.13348 \[hep-ph\]](#).
- [44] J.-C. Yu, Y. Cao, Y. Tang, and Y.-L. Wu, [Phys. Rev. D **110**, 023025 \(2024\)](#), [arXiv:2404.04333 \[hep-ph\]](#).
- [45] Y.-H. Yao and Y. Tang, (2024, [Phys. Rev. D in press](#)), [arXiv:2404.01494 \[hep-ph\]](#).
- [46] P. A.-S. et al, “[Laser interferometer space antenna](#),” (2017), [arXiv:1702.00786 \[astro-ph.IM\]](#).
- [47] W.-R. Hu and Y.-L. Wu, [Natl. Sci. Rev. **4**, 685 \(2017\)](#).
- [48] J. L. et al, [Classical and Quantum Gravity **33**, 035010 \(2016\)](#).
- [49] J. Crowder and N. J. Cornish, [Phys. Rev. D **72**, 083005 \(2005\)](#), [arXiv:gr-qc/0506015](#).
- [50] S. M. Carroll, G. B. Field, and R. Jackiw, [Phys. Rev. D **41**, 1231 \(1990\)](#).
- [51] S. M. Carroll and G. B. Field, [Phys. Rev. D **43**, 3789 \(1991\)](#).
- [52] D. Harari and P. Sikivie, [Phys. Lett. B **289**, 67 \(1992\)](#).
- [53] A. Khmelnitsky and V. Rubakov, [Journal of Cosmology and Astroparticle Physics **2014**, 019 \(2014\)](#).
- [54] L. Hui, [Ann. Rev. Astron. Astrophys. **59**, 247 \(2021\)](#), [arXiv:2101.11735 \[astro-ph.CO\]](#).
- [55] M. Tinto and S. V. Dhurandhar, [Living Rev. Rel. **24**, 1 \(2021\)](#).
- [56] J. W. Foster, Y. Kahn, R. Nguyen, N. L. Rodd, and B. R. Safdi, [Phys. Rev. D **103**, 076018 \(2021\)](#).
- [57] M. Lisanti, M. Moschella, and W. Terrano, [Phys. Rev. D **104**, 055037 \(2021\)](#).
- [58] A. V. Gramolin, A. Wickenbrock, D. Aybas, H. Bekker, D. Budker, G. P. Centers, N. L. Figueroa, D. F. Jackson Kimball, and A. O. Sushkov, [Phys. Rev. D **105**, 035029 \(2022\)](#).
- [59] D. W. P. Amaral, M. Jain, M. A. Amin, and C. Tunnell, [JCAP **06**, 050 \(2024\)](#), [arXiv:2403.02381 \[hep-ph\]](#).
- [60] B. Saleh and M. Teich, [Fundamentals of Photonics, 3rd Edition \(2019\)](#).
- [61] W. DeRocco and A. Hook, [Phys. Rev. D **98**, 035021 \(2018\)](#).
- [62] S. Babak, M. Hewitson, and A. Petiteau, “[Lisa sensitivity and snr calculations](#),” (2021), [arXiv:2108.01167 \[astro-ph.IM\]](#).

- [63] V. Corbin and N. J. Cornish, *Class. Quant. Grav.* **23**, 2435 (2006), [arXiv:gr-qc/0512039](#).
- [64] G. P. Centers *et al.*, *Nature Commun.* **12**, 7321 (2021), [arXiv:1905.13650 \[astro-ph.CO\]](#).
- [65] A. Payez, C. Evoli, T. Fischer, M. Giannotti, A. Mirizzi, and A. Ringwald, *Journal of Cosmology and Astroparticle Physics* **2015**, 006 (2015).
- [66] S. K. et al, *Classical and Quantum Gravity* **23**, S125 (2006).
- [67] W. Martens, M. Khan, and J.-B. Bayle, *Classical and Quantum Gravity* **40**, 195022 (2023).
- [68] W.-T. NI, *International Journal of Modern Physics D* **22**, 1341004 (2013), <https://doi.org/10.1142/S0218271813410046>.
- [69] G. M. Harry, P. Fritschel, D. A. Shaddock, W. Folkner, and E. S. Phinney, *Class. Quant. Grav.* **23**, 4887 (2006), [Erratum: *Class.Quant.Grav.* 23, 7361 (2006)].
- [70] I. Irastorza *et al.* (IAXO), (2013).
- [71] J. Gué, A. Hees, and P. Wolf, “Probing the axion-photon coupling with space-based gravitational waves detectors,” (2024), [arXiv:2410.17763 \[hep-ph\]](#).